Paleoceanography and Paleoclimatology

RESEARCH ARTICLE
10.1029/2020PA004182

Key Points:

- First high-resolution relative nutrient utilization record during Late Pliocene from Arctic
- Relative nutrient utilization is related to stratification at the study site
- Stronger (weaker) stratification found during warm (cold) periods of the Late Pliocene

Supporting Information:

Supporting Information may be found in the online version of this article.

Correspondence to:

M. Tiwari,
manish@ncpor.res.in

Citation:

Behera, P., Tiwari, M., & Knies, J. (2021). Enhanced Arctic stratification in a warming scenario: Evidence from the Mid Pliocene warm period. *Paleoceanography and Paleoclimatology*, *36*, e2020PA004182. https://doi.org/10.1029/2020PA004182

Received 7 DEC 2020
Accepted 25 MAY 2021

Enhanced Arctic Stratification in a Warming Scenario: Evidence From the Mid Pliocene Warm Period

Padmasini Behera[1,2], Manish Tiwari[1], and Jochen Knies[3,4]

[1]National Centre for Polar and Ocean Research, Ministry of Earth Sciences, Vasco-da-Gama, Goa, India, [2]School of Earth, Ocean and Atmospheric Sciences, Goa University, Goa, India, [3]Geological Survey of Norway, Trondheim, Norway, [4]CAGE – Centre for Arctic Gas Hydrate, Environment and Climate, UiT The Arctic University of Norway, Tromsø, Norway

Abstract Global warming is most pronounced in the Arctic as evident from the massive sea ice loss during the past few decades. The Mid-Pliocene Warm Period (MPWP), 3.264 – 3.025 million years ago with similar CO_2 levels, is the nearest analogue for understanding the impacts of future global warming. High-resolution studies of relative nutrient utilization and productivity from the Atlantic-Arctic Gateway (AAG) can provide insight into the nutrient availability governed by stratification strength during past warm climates. Here, we present relative nutrient utilization and productivity variability during the MPWP using sediments collected during the Ocean Drilling Program (ODP) Leg 151 from Fram Strait, AAG. We find that the relative nutrient utilization was high (low) implying stronger (weaker) stratification during warm (cold) periods during the MPWP. Stronger stratification inhibits the nutrient influx from intermediate water depths into the surface leading to higher utilization of available nutrients. It existed during warm periods likely due to enhanced summer sea ice melt and river discharge from the hinterland. As a consequence, the freshened surface layer could have stored more heat and accelerated the sea ice melt further implying that in the present-day warm scenario, stronger stratification and upper layer freshening may lead to more sea ice melt in the Arctic Ocean.

1. Introduction

Global warming is expected to be most pronounced in the polar regions, which is seen most dramatically in the Arctic Ocean with significant sea ice loss over the last few decades (Cavalieri & Parkinson, 2012). The sea ice regulates various factors such as surface albedo, ocean-atmosphere heat exchange, and potential freshwater export to the North Atlantic. This in turn influences the deep-water formation in the North Atlantic and global ocean circulation (Sévellec et al., 2017). Recent studies using mooring data and models suggest the oceanic heat input via advective inflow of warm North Atlantic Current (NAC) and Pacific waters into the Arctic Ocean plays a major role in sea ice melting (Pnyushkov et al., 2015). This scenario is seen in the eastern Eurasian Basin, where the NAC interacts with surface waters and weakens the stratification, thereby contributing to the sea ice melt (Onarheim et al., 2014). However, the enclosed Arctic Ocean receives a huge amount of freshwater from the Circum-Arctic river discharge (11% of the global river discharge, Gleick, 2000) and precipitation (Rudels et al., 1991). This large volume of freshwater influx contributes to additional heat input by strengthening the upper water column stratification, which reduces the sea ice cover (Carmack et al., 2015). Alternatively, the stratified water column also prevents the sea ice from melting by inhibiting the vertical mixing of warm Atlantic water with the surface layer (Aagaard et al., 1981). Hence, knowledge of past variability of stratification during analogous warm periods may help in understanding the significance of stratification in the melting of sea ice in the Arctic Ocean.

To improve our understanding of the impact of a warmer climate on Arctic stratification, past climates with similar boundary conditions need to be examined. Such an opportunity is presented by the Mid-Pliocene Warm Period (MPWP, 3.264 – 3.025 Ma, million years ago; Dowsett et al., 2009; Dowsett et al., 2019; Haywood et al., 2020), which is the most recent such event when the conditions were similar to the present with similar CO_2 concentration (365 – 415 ppmv, Berends et al., 2019; Bartoli et al., 2011), a sea-level higher by approximately 20 m than the present (Rohling et al., 2014), and annual mean surface temperature higher by 2.7°C – 4.0°C (Haywood et al., 2013). Earlier studies on MPWP have shown that the sea ice coverage at the Atlantic-Arctic Gateway (AAG) region reduced considerably (Cronin et al., 1993; Rahaman

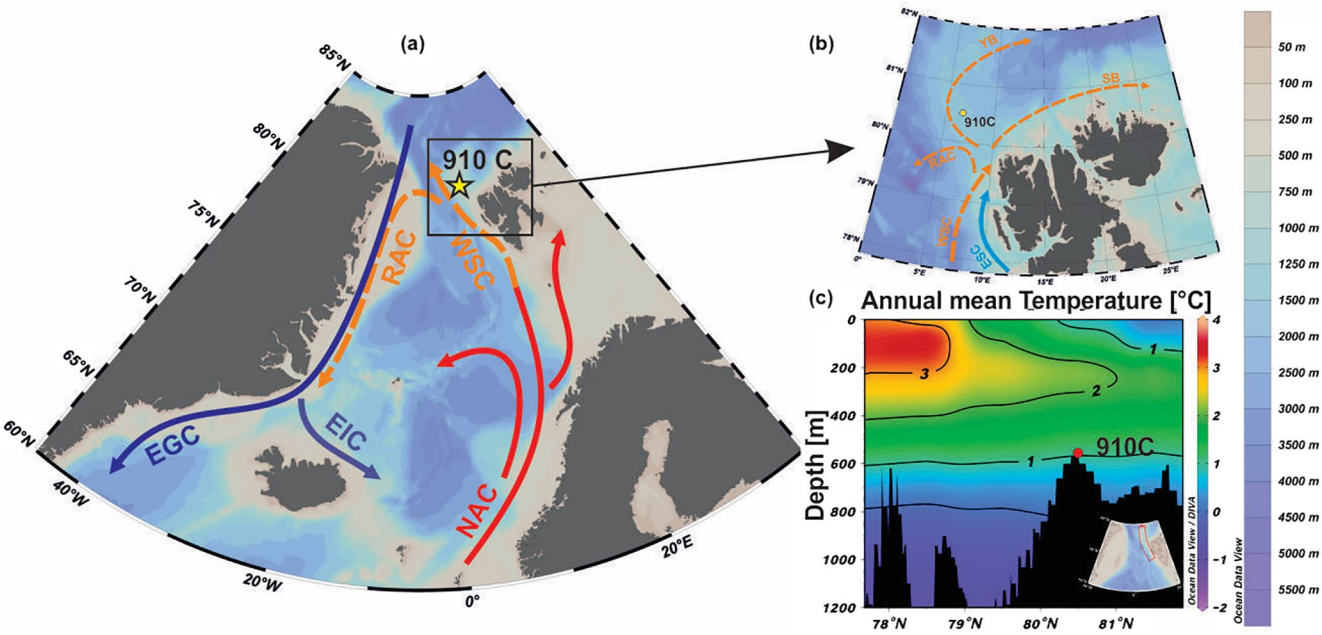

Figure 1. Sampling location. (a) Location of sampling site 910C (80° 15.896′N, 6° 35.430′E) shown as a star. The Norwegian Current transports North Atlantic warm water from 60°N to the Arctic region. RAC - Return Atlantic Current, WSC - West Spitsbergen Current, NAC - North Atlantic Current, EIC - East Icelandic Current, EGC - East Greenland Current. Surface and subsurface water are shown by solid and dotted lines respectively; (b) The warm and saline NAC circulation at the Yermak Plateau. ESC - East Spitsbergen Current, YB - Yermak Branch, SB - Svalbard Branch; (c) Profile of mean annual temperature at the Yermak Plateau; the core location is marked as red dot and the inset shows the transect.

et al., 2020). Other studies, though at a coarser resolution or spanning only a few glacial-interglacial cycles, noted that the oceanic circulation/ventilation at the AAG reduced (enhanced) during colder (warmer) periods (Dowsett et al., 1992; Ravelo & Andreasen, 2000). The model simulations also observed that the Atlantic Meridional Overturning Circulation (AMOC) was stronger with enhanced oceanic heat transport to the polar region during the MPWP (Otto-Bliesner et al., 2017; Zhang et al., 2020). Despite the above advances, high-resolution (multi-millennial scale) studies on various facets of circulation at the AAG including water column stratification for the MPWP are lacking. Here, we aim to understand changes in Arctic stratification during glacial and interglacials of MPWP by studying the relative nutrient utilization and productivity from the Yermak Plateau, AAG (Figure 1a).

Water column stratification in higher latitudes can be constructed using the relative nutrient utilization variability inferred from the nitrogen isotopic composition ($\delta^{15}N$) of sedimentary organic matter (Thibodeau et al., 2017). In polar and subpolar regions, the nitrogen isotopic value of the settling organic matter is controlled by the degree of nutrient utilization (Schubert & Calvert, 2001). In the photic zone, the phytoplankton preferentially uptake the lighter ^{14}N-nitrate over the heavier ^{15}N-nitrate, provided nitrate uptake is incomplete. Under nitrate replete conditions (low relative nutrient utilization), the settling particulate organic matter is depleted in the heavy isotope (low $\delta^{15}N$). While under nitrate poor conditions (high relative nutrient utilization), the phytoplankton consumes a relatively higher amount of ^{15}N-nitrate resulting in high $\delta^{15}N$ (Altabet & Francois, 1994). In the Arctic Ocean, the nutrient concentration at the surface is controlled by the mixed layer thickness and thus by the stratification of the upper water column (Codispoti et al., 2013). The stronger stratification in the Arctic Ocean during spring and summer (growth season) limits the nitrate to the photic zone, resulting in maximum consumption of nutrients at the surface. This leads to high relative nutrient utilization and thus the settling organic particles are isotopically heavier (high $\delta^{15}N$) (Thibodeau et al., 2017). The major nutrient source to the Arctic Ocean is advective nutrient input via Atlantic and Pacific entrances (Torres-Valdes et al., 2013). Nutrient inputs from the river and sea ice melt are small (1.46 – 1.7 kmol nitrate s^{-1}) in comparison to the advective inputs (~52 kmol nitrate s^{-1} through Fram Strait) (Torres-Valdes et al., 2013). The $\delta^{15}N$ values can indicate relative nutrient utilization related to mixed

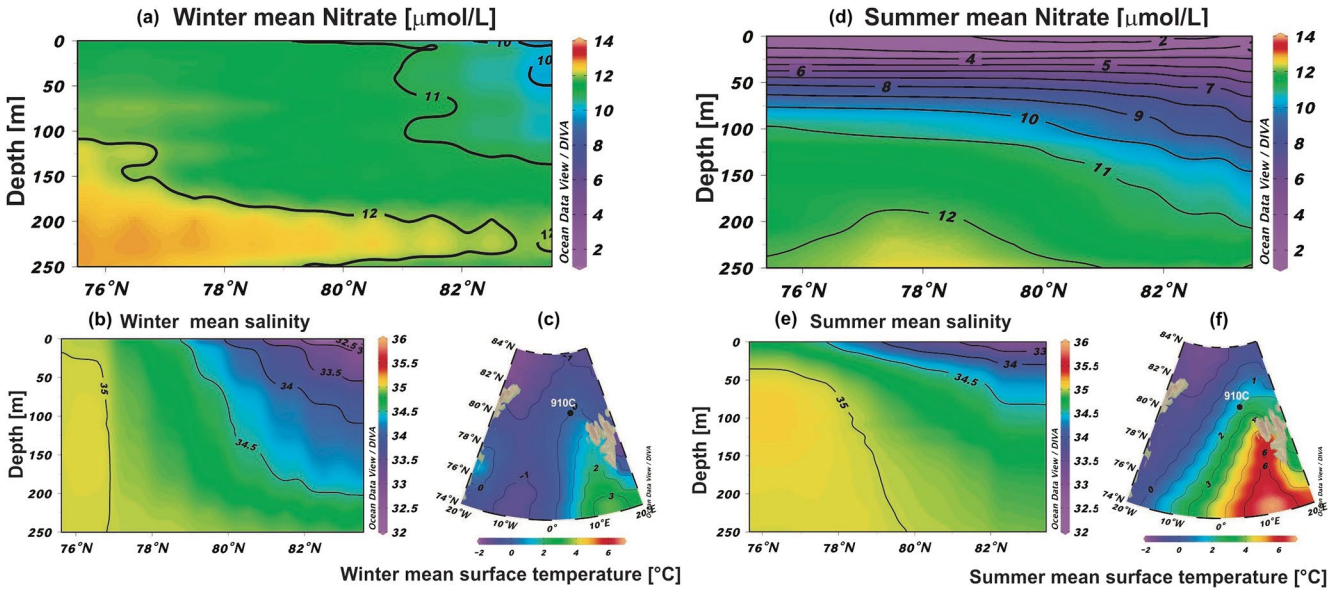

Figure 2. Modern oceanographic conditions (a), (d) Profile of nitrate concentration variability during modern winter and summer periods at the sample location; (b), (c), (e), and (f) profile of modern winter and summer mean salinity and temperature variability at the study site. The black dot shows the sampling location (c) and (f) and the section track is given in the Supplementary Information.

layer depth and hence, the mixing of nutrient-rich Atlantic water with the surface. We use this approach of temporal variation in nitrate utilization to study the past stratification at the Ocean surface at Fram Strait.

2. Modern Oceanography at the Study Site

ODP Hole 910C is located at 80°15.896′N, 6°35.430′E in southern Yermak Plateau at a water depth of 556.4 m. The NAC feeds the Norwegian Current which in turn supplies water to the West Spitsbergen Current (WSC) (Figures 1a and 1b). The WSC transports the relatively warm (>3°C) and saline (>35.0) North Atlantic water into the Arctic Ocean (Figures 1b and 1c; Beszczynska-Mller, 2012). The WSC supplies heat to the eastern Fram Strait making it the northernmost perennially ice-free sea area in the world (Haugan, 1999). Cold and relatively low salinity water, carrying on an average approximately 1,300 km^3 of freshwater, annually outflows from the Arctic Ocean via the East Greenland Current (EGC) (de Steur et al., 2009). The heat transport to the Arctic Ocean through NAC along eastern Fram Strait varies seasonally. The core site experiences ~2°C warmer temperature during the summer period than during the winter period (Figures 2c and 2f). The sensitivity of the seawater density to the temperature reduces in the polar region as it reaches the freezing point and thus, the stratification in the Arctic Ocean is primarily due to the salinity gradient in the water column (Adkins et al., 2002). Based on salinity distribution, the Arctic Ocean water column is separated into three different layers (Rudels et al., 1991). The polar surface layer extends from ~0 to 250 m depth, which consists of the Polar Mixed Layer (PML) and the halocline. The PML comprises fresh and cold water from the Pacific Ocean, river runoff, an excess of precipitation over evaporation, and sea ice melt (Nummelin et al., 2016). The cold halocline (~50 – 250 m depth), which has an advective origin, separates the cold and fresh surface water from warm and saline intermediate Atlantic water (Rudels et al., 1991; Rudels, 2015). In the Eurasian Basin, this layer is formed by the advection of higher saline Atlantic water along the shelves to the deeper basin (Coachman & Barnes, 1962). The warm and saline water in the intermediate layer (~400 – 600 m depth) is advected from the north Atlantic to the Arctic Ocean and descends beneath the surface layer in the Nansen Basin, from where it supplies nutrient to the surface through diapycnal mixing (Rudels et al., 1991; Randelhoff et al., 2015). During summer, the surface water is well stratified with a mixed layer thinner than 30 m (Figures 2d and 2e), which results in low nitrate concentration (2 – 4 μmol/L) at the polar mixed layer during this period (Figure 2d). In winter, the sea ice formation, brine rejection, and haline convection promote the deeper mixing, which creates the PML thickness up to ~250 m depth (Figures 2a and 2b). The deeper mixing allows for the replenishment

Table 1
The Tie-Points for the Chronology are From the Knies et al., 2014 and are Derived Using Oxygen Isotope Stratigraphy (Lisiecki & Raymo, 2005), Magnetostratigraphy (Lourens et al., 2005), and Biostratigraphy (Sato & Kameo, 1996)

Age (Ma)	910C (mbsf)	Sedimentation rate (cm/kyr)	Datum	Source
2.438	153.38		MIS 96[a]	Lisiecki and Raymo, 2005
2.510	171.00	24.5	MIS 100 Top	Lisiecki and Raymo, 2005
2.540	175.70	15.7	MIS 100 Base	Lisiecki and Raymo, 2005
2.565	184.67	35.9	MIS 102[a]	Lisiecki and Raymo, 2005
2.645	204.48	24.8	MIS G2[a]	Lisiecki & Raymo, 2005
2.830	223.00	10.0	"Datum A"	Sato and Kameo, 1996
3.295	260.40	8.0	MIS M2	Lisiecki and Raymo, 2005
3.596	305.00	14.8	Gauss/Gilbert	Lourens et al., 2005

Abbreviation: MIS, Marine Isotope Stage.
[a]means age of heaviest $\delta^{18}O$ value within respective MIS is considered.

of nutrients at the surface and thus, the nitrate concentration is higher ~11 μmol/L at the surface during winter in comparison to the summer period (Figure 2a).

3. Materials & Methods

3.1. Study Site and Age-Depth Model

The 507.4 m long sediment core was raised from 556.4 m water depth in the southern part of Yermak Plateau (80°15.896′N, 6°35.430′E) and out of which 199.2 – 276.2 m is used in the present study pertaining to the late Pliocene. The chronology of the core is constructed using the tie points as given in Table 1 (Figure S2) and described in detail elsewhere (Rahaman et al., 2020). The age range of these samples is from 2.6 to 3.4 Ma that encompasses the MPWP.

3.2. Relative Nutrient Utilization and Provenance

The relative nutrient utilization is determined from the nitrogen isotopic ratio of organic matter ($\delta^{15}N_{org}$). The provenance of organic matter is determined through a cross-plot between the total organic carbon to total nitrogen ratio (TOC/TN) and $\delta^{13}C$ values of organic matter ($\delta^{13}C_{org}$). We analyzed these parameters from sediments collected from Hole 910C. Around 3 g of freeze-dried sample was ground finely for the homogenization before nitrogen and carbon isotopic ratio ($\delta^{15}N$ and $\delta^{13}C$) and total nitrogen and total organic carbon concentration analysis of the sedimentary organic matter. The homogenized samples were divided into two sub-samples for two different analyses–(a) samples were treated with 2N HCl for TOC and $\delta^{13}C$ measurement, and (b) untreated samples were used for TN concentration and $\delta^{15}N$ analysis because acid treatment has been reported to affect the nitrogen content and isotopic values of the sedimentary organic matter (SOM) (Brodie et al., 2011). The acid treatment removed inorganic carbon from the sediment allowing analysis of TOC and $\delta^{13}C$ of the organic matter. 20 ml of freshly prepared 2N HCl was added to 1 – 2 g finely ground sediment. The solution was shaken mechanically and kept overnight. After the full settlement of the sediments to the bottom of the beaker, the acid was decanted from the sample. The sample was washed with ultrapure demineralized water until its pH became neutral. Approximately, 5 mg of treated sediment sample was taken for the $\delta^{13}C$ and TOC measurement whereas for $\delta^{15}N$ and TN analysis, around 120 g of bulk ground sediment was used. The isotopic analysis and elemental concentration were measured by an Isoprime Isotope Ratio Mass Spectrometer coupled with an Elemental Analyzer (Vario Isotope Cube) in Marine Stable Isotope Lab of National Center for Polar and Ocean Research, Goa, India. In the case of $\delta^{13}C$ and TOC, alternate samples were analyzed. The isotopic values are expressed in delta (δ) notation, which is the relative difference of isotopic ratios in the sample from an international standard. Thus, in the case of nitrogen isotopes: $\delta^{15}N = \{(^{15}N/^{14}N)_{sample}/(^{15}N/^{14}N)_{standard}\}-1$; where $(^{15}N/^{14}N)_{sample}$ and $(^{15}N/^{14}N)_{standard}$ are the ratios of the abundances of the less abundant (heavier, *i.e.*, ^{15}N) to more abundant (lighter, *i.e.*, ^{14}N)

isotope in the sample and standard, respectively. The $\delta^{15}N$ and $\delta^{13}C$ values are multiplied by 10^3 and are expressed in per mil (‰). The uncertainties for the $\delta^{15}N$ and $\delta^{13}C$ analysis are ±0.24‰ and ±0.18‰, respectively, based on repeated measurement of the standard reference material IAEA-N1 (ammonium sulphate, $n = 43$) and IAEA-600 (Caffeine, $n = 27$). Similarly, the uncertainties for TN and TOC are ±0.81% ($n = 81$) and ±0.80% ($n = 56$), respectively, determined using Sulfanilamide as standard.

4. Results and Discussion

4.1. Provenance of Sedimentary Organic Matter and no Alteration of $\delta^{15}N$

The provenance of SOM is determined from both the C/N ratio and $\delta^{13}C$ values of the SOM. The average $\delta^{13}C$ value of the marine and terrestrial (C3 plant) organic matter is −21‰ and −27‰, respectively (Ruttenberg & Goñi, 1997). Most of the $\delta^{13}C$ values observed in the present study are near the marine end-member. The C/N ratio of SOM is also widely used to determine the provenance of organic matter. The C/N ratio of marine organic matter ranges from 8 to 10 while it ranges from 20 to 100 in the case of terrestrial organic matter (Meyers, 1994). The higher values of C/N ratio in the terrestrial organic matter are due to the presence of low nitrogen and high carbon content compounds like lignin and cellulose found in the plant cell wall. In the present study, the C/N ratio of the SOM varies from 8 to 12. We further plotted $\delta^{13}C$ versus C/N ratio to determine the provenance (Figure S3). It shows that most of the values are near the marine end-member, so the SOM appears to be mostly of marine origin with a little contribution from the terrestrial organic matter. Myhre et al., 1995, in the initial proceedings of ODP 151, have also shown that the origin of organic matter from 160 to 380 mbsf (meter below seafloor) is predominantly from the marine environment. Nevertheless, to check the effect of the terrestrial organic matter on the $\delta^{15}N$ of the SOM, we plotted $\delta^{15}N$ versus $\delta^{13}C$ (Figure S4a). The $\delta^{15}N$ values of the terrestrial and marine organic matter are ∼4‰ and around 5 – 7‰ respectively (Sigman et al., 2009). Thus, both the $\delta^{15}N$ and $\delta^{13}C$ values of the terrestrial organic matter are lower than the marine counterpart. Hence, if there is any effect of the terrestrial contribution on the $\delta^{15}N$ of the SOM, it should yield a positive correlation between $\delta^{15}N$ and $\delta^{13}C$ of the SOM. In the present study, we do not find any correlation between $\delta^{15}N$ and $\delta^{13}C$ ($r^2 = 0.01$) of SOM (Figure S4a) confirming that the terrestrial contribution does not affect the $\delta^{15}N$ values of SOM significantly.

Additionally, the degree of sedimentary $\delta^{15}N$ alteration is a function of oxygen exposure time during the early burial stage (Robinson et al., 2012). The oxygen exposure time is linearly related to the water column depth and sedimentation rate. The time of exposure is generally prolonged in deep-sea due to the slow sedimentation rate. But, in the present study, the water depth is only 556.4 m with a high sedimentation rate (8 – 24 cm/kyr). So, no diagenetic alteration is expected. Still, we checked whether diagenesis has affected the $\delta^{15}N$, TOC, and TN values in the present study. Diagenetic activity increases the $\delta^{15}N$ values while reduces the TOC and TN concentration (Freudenthal et al., 2001). Therefore, if diagenesis has taken place then the $\delta^{15}N$ should exhibit anti-covariance with TOC and TN and covariance with C/N ratio (Tripathi et al., 2017). We do not find any correlation between $\delta^{15}N$ versus TOC, TN, and C/N ($r^2 = 0.03$, 0.002, and 0.006) (Figures S4b–S4d) implying there is no effect of diagenetic degradation on SOM in the sediment used in the present study.

4.2. Stratification During Mid-Pliocene Interglacial Periods

The MPWP spans 3.264 – 3.025 Ma which has three major warm periods MIS KM5 (3.20 – 3.19), KM3 (3.18 – 3.16 Ma), and K1 (3.09 – 3.06 Ma) (Haywood et al., 2013; Lisiecki & Raymo, 2005, Figure 3a). Two other interglacials i.e., MIS G7 (2.78–2.74 Ma) and MIS G3 (2.7 – 2.66 Ma) follow the MPWP. During these interglacials, the $\delta^{15}N$ values of the organic matter vary between 5.0‰ and 5.7‰ (Figure 3b). The surface water productivity inferred from $CaCO_3$ content and the mass accumulation rate of $CaCO_3$ ($CaCO_3$-MAR) shows an increasing trend during these interglacial periods (Figure 3d). The trace element Ba occurs as barite ($BaSO_4$) in the marine environment related to the organic carbon flux. Barite has higher preservation compared to other productivity proxies like $CaCO_3$ and TOC (Dymond et al., 1992; Gingele et al., 1999). Therefore, Ba is considered as a good proxy for ocean productivity. However, usually, Ba-excess is used, which is the fraction of Ba that is not supplied by terrigenous material and is determined by normalizing Ba by Al.

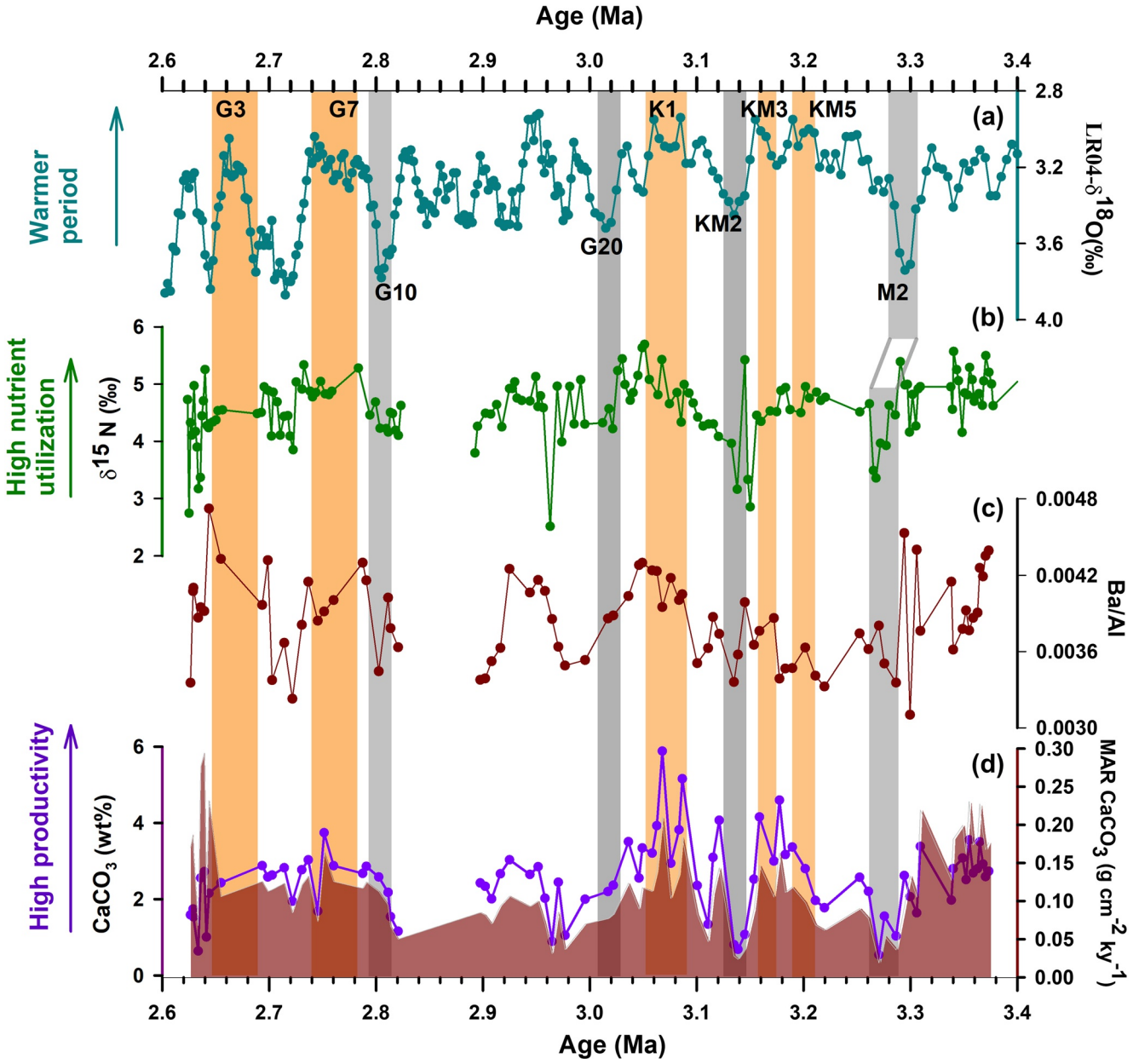

Figure 3. Relative nutrient utilization and productivity variability during late Pliocene. (a) LR04 stack of $\delta^{18}O$ (‰) of benthic foraminifera (Lisiecki & Raymo, 2005); (b) $\delta^{15}N$ (‰) representing the relative nutrient utilization during different periods; (c) and (d) Ba/Al, $CaCO_3$ (%) and Mass Accumulation Rate of $CaCO_3$ showing the paleoproductivity variability. Gray bands indicate colder periods while the colored bands show warmer periods. Positions of Marine Isotope Stages M2, KM3, KM2, K1G20, G10, G7, and G3 are shown.

During interglacials, the open surface water together with nutrient-rich meltwater supply and high river discharge led to higher productivity as recorded by an increase in Ba/Al ratio, the $CaCO_3$ content, and its MAR (Figures 3c and 3d). However, the increase in $\delta^{15}N$ values during interglacials indicates high relative nutrient utilization suggesting higher consumption of the available nutrients (Altabet & Francois, 1994; Schubert & Calvert, 2001). The enhanced productivity during the warmer periods due to sufficient light availability utilizes more of the available nutrient causing high relative nutrient utilization (high $\delta^{15}N$ values) (Knies et al., 2007; Randelhoff et al., 2015). Additionally, the high relative nutrient utilization suggests that mixing with the deeper nutrient-rich waters was reduced significantly. Similar enrichment of $\delta^{15}N$ values is found in both the central Arctic Ocean during the Holocene (5‰ – 6.8‰, Schubert et al., 2001) and the subpolar region during MIS 5e and MIS 11 interglacials (4.8‰ and 5.2‰, Thibodeau et al., 2017). This

increase in relative nutrient utilization during warmer periods is attributed to lower nutrient conditions because of a thinner surface mixed layer due to enhanced stratification. This inference corroborates modern summer observations where the surface nitrate concentration appears to be low in the study region (Figure 2d). The reduction of the surface mixed layer is supported by the instrumental data (30 years) from the Arctic Ocean, which indicates a shoaling of the mixed layer in the order of 0.5 – 1 m/year and thus increased water mass stratification (Peralta-Ferriz & Woodgate, 2015). The low saline surface waters are well separated from the deep waters causing a restriction in nutrient exchange (Figures 2d and 2e) and thus high nutrient utilization manifested through high $\delta^{15}N$ (5‰ – 7‰) values in surface sediments (Knies et al., 2007; Schubert & Calvert, 2001). Hence, we propose that high $\delta^{15}N$ values during interglacials observed in Hole 910C likely suggest enhanced stratification during warmer periods during the MPWP in the AAG.

The factors that melt sea ice are both the summer solar heating (Perovich et al., 2011) and the inflow of warm water from both the Pacific and Atlantic Ocean (Carmack et al., 2015; Polyakov et al., 2017). Data from ODP holes 909A and 911A indicate that despite discrepancies in sea surface temperatures (SST) values ranging from 12°C to 18°C, both records show generally higher SSTs at Yermak Plateau during the late Pliocene compared to the present (Knies et al., 2014; Robinson, 2009). The data also corroborates observations from the North Atlantic region (ODP 982) suggesting an increase of SST during warmer periods of MPWP (Figure 4d; Lawrence et al., 2009). The warmer and open water conditions during this period at the study site are also supported by summer sea ice-free conditions inferred from reduced abundance of sea ice proxy IP_{25}, and open water proxy HBI III (Figure 4c) as well as less influx of ice-rafted debris (Figure 4f) (Knies et al., 2002, 2014; Rahaman et al., 2020). Another earlier study observed ice-free summers, and probably a perennially ice-free Arctic Ocean during the MPWP due to the inflow of warm Atlantic water into the Arctic Ocean through the Fram Strait (Cronin et al., 1993). A recent high-resolution study from the same site (910C, Yermak Plateau) found less radiogenic neodymium isotope (low ε_{Nd}) during warmer periods of MPWP (Figure 4b) indicating a significant inflow of warm and saline Atlantic water into the Arctic (Rahaman et al., 2020). Comparison of ε_{Nd} and $\delta^{15}N_{org}$ suggests that the enhanced NAC to the Arctic could have played a major role in strengthening the stratification which led to high relative nutrient utilization (Figures 4a and 4b). This enhanced NAC transported heat to the polar region, which could have amplified the Arctic temperature during MPWP (Dowsett et al., 1992). The warmth caused an increase in the river runoff, sea ice melt, and precipitation during interglacials, which could have strengthened the stratification during MPWP further. We propose that the higher sea ice melt and freshwater influx along with enhanced NAC during warmer periods of MPWP including MIS G3 and G7 would have contributed to the enhanced stratification at the Yermak Plateau (shown pictorially in Figure 6a).

4.3. Stratification During Mid-Pliocene Glacial Periods

The increase in $\delta^{18}O$ value from 3.1‰ to 3.7‰ (Lisiecki & Raymo, 2005) between 3.33 and 3.31 Ma marks the colder event termed as MIS M2 glacial period (Figure 3a). It is a large global glaciation that lasted for 50 kyr and interrupted the trend of global warming at 3.3 Ma. One hypothesis to explain the cooling is that the opening of the Central American Seaway (CAS) resulted in the weakening of the AMOC and NAC leading to less heat transport towards the polar region causing the M2 glaciation (De Schepper et al., 2013). Tan et al., 2017, suggests that the opening of CAS helps in the reduction of northward heat transport but can not alone explains the onset of M2 glaciation. They proposed that the reasons for the M2 glaciation were the presence of the shallow open CAS with other factors like favorable orbital parameters, decrease in CO_2 concentration (220 ppmv), vegetation albedo, and ice sheet feedback that led to the sea ice buildup in northern high latitudes. In the present study, the MIS M2 glacial period corresponds to the lower $\delta^{15}N$ value (shown by the tilted gray band in Figure 3), which decreased from 5.4‰ to 3.4‰. An exact match at M2 is not observed, possibly, due to the different chronologies of the LR04 and our record and their inherent chronological errors. The high $\delta^{15}N$ values observed at 3.3 Ma could be the result of interglacial before M2 glacial period. Other glacial periods (i.e., KM2, G20, and G10) are also marked by the increase in $\delta^{18}O$ values and low $\delta^{15}N$ values (Figure 3b). Surface water productivity indicators ($CaCO_3$, $CaCO_3$ MAR, and Ba/Al) decreased to a minimum during these colder periods (Figures 3c and 3d). The enhanced sea ice cover during these colder periods could have caused light limitations and hence lower surface productivity compared to interglacial periods. The low $\delta^{15}N$ values during these colder periods represent low relative nutrient utilization at the Yermak Plateau implying eutrophic conditions and potentially a thickening of the polar

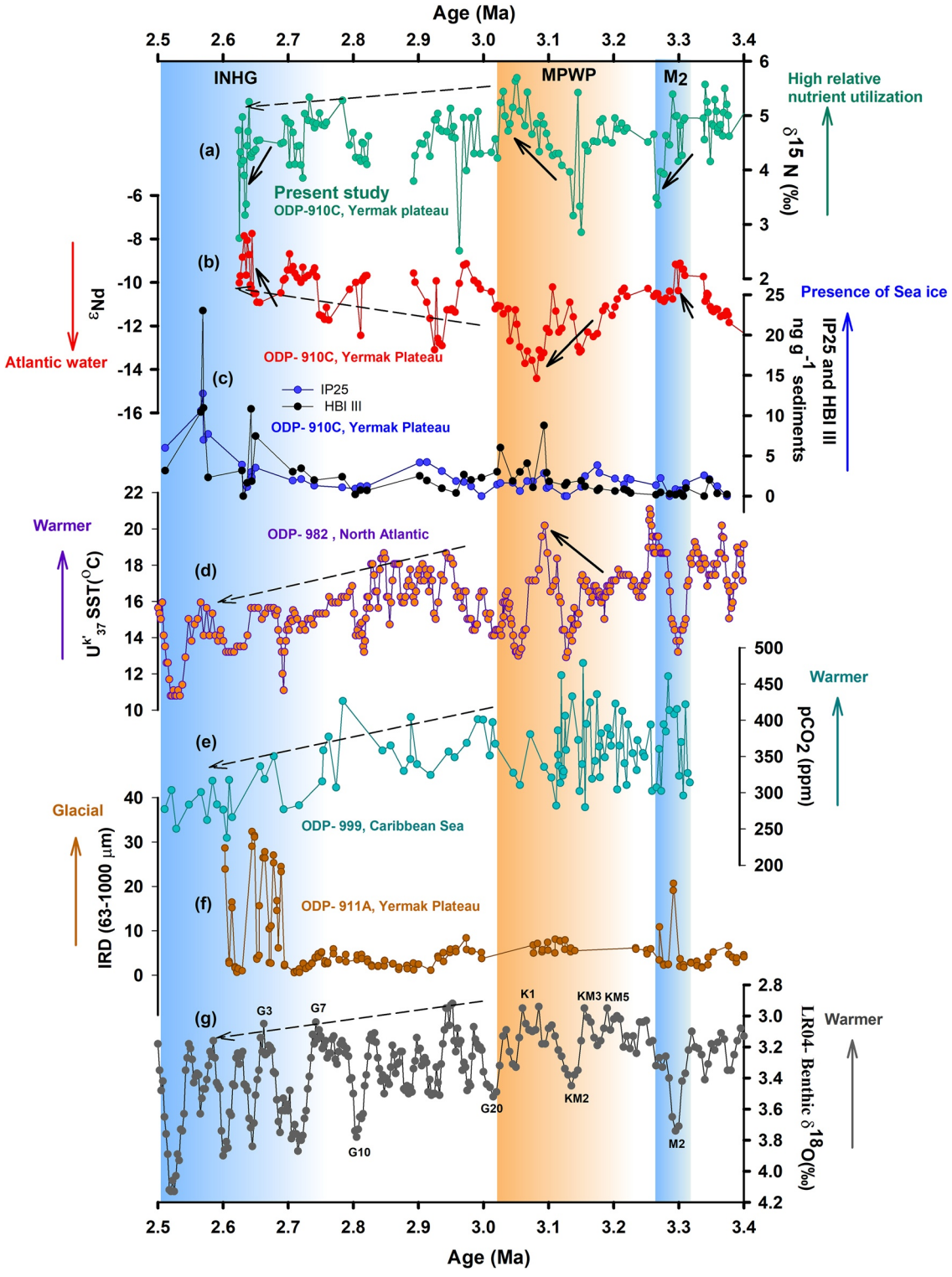

Figure 4. Comparison of relative nutrient utilization with sea surface temperature (SST), Atlantic water inflow, and sea ice extent. (a) $\delta^{15}N$ record from ODP-910C (present study) shows the relative nutrient utilization; (b) and (c) Authigenic ε_{Nd} record and sea ice proxy (IP_{25}) with open water biomarker Highly Branched Isoprenoid III from 910C (Rahaman et al., 2020); (d) SST record from the ODP Site 982 (North Atlantic) using Alkenone UK_{37} (Lawrence et al., 2009); (e) Atmospheric CO_2 concentration reconstructed using $\delta^{11}B_{borate}$ of *G. ruber* from ODP site 999, Caribbean Sea (de la Vega et al., 2020); (f) IRD record from the ODP Site 911A (Yermak Plateau, Knies et al, 2014); (g) LR04 stack of $\delta^{18}O$ (‰) of benthic foraminifera (Lisiecki & Raymo, 2005). Dashed arrows show long term trend from 3.1 to 2.6 ma and solid arrow indicates glacial-interglacial trends.

mixed layer causing mixing with nutrient-rich water (Rudels et al., 1991). Schubert et al., 2001 also reported low relative nutrient utilization (low $\delta^{15}N$) and low productivity due to the perennial sea ice cover during the Last Glacial Maximum (LGM) in the central Arctic Ocean. It suggests the replenishment of nutrients at the surface is due to the low stratification and enhanced mixing of deep-water nitrate source. The high nitrate concentration in the surface water is also supported by the observations during the modern winter period where nitrate concentration reaches up to 11 μmol/L with a low salinity gradient at the study site (Figure 2a).

Hence, we suggest that during the glacial periods of the MPWP, the reduction of Atlantic water inflow into the Arctic Ocean expressed by high ε_{Nd}, values (Figure 4b; Rahaman et al., 2020) are likely responsible for the weaker stratification of the surface waters. We postulate that the associated enhanced sea ice formation reduced the stratification and increased the mixing thickness of PML during the colder periods of MPWP leading to less nutrient utilization (shown pictorially in Figure 6b).

On considering the long-term trends from ~3.0 to 2.6 Ma (dashed arrows in Figure 4), we note a reduction of CO_2 concentration (de la Vega et al., 2020, Figure 4e) and SST at the Atlantic Ocean (Figure 4d) representing a long-term cooling. This long-term cooling coincides with the reduction of NAC inflow to the Arctic Ocean as evident from the gradual increase in ε_{Nd} values at the Yermak Plateau (Figure 4b). The cooling matches with the modest decrease in $\delta^{15}N$ values of SOM towards INHG, which indicates the decrease in relative nutrient utilization and thus low stratification at AAG. Thus, the changes that occurred during the individual glacial periods match with the changes occurring during the long-term increase in glaciation.

4.4. Forcing Factor of the Arctic Stratification

Stratification in the Arctic Ocean is governed by both sea ice dynamics and river discharge. These could have been affected by both internal (i.e., Ocean-Atmosphere interactions, land-air interaction, and atmospheric internal dynamics) as well as external forcings (i.e., orbital). To identify the forcing factors of the Arctic stratification, we compared the relative nutrient utilization with the eccentricity as well as the solar insolation variability in the Northern hemisphere during the summer season (from 65°N and July month) (Figure 5a). We find that strong stratification (high $\delta^{15}N$ values) coincides with strong solar radiation and high eccentricity. We also carried out the spectral analysis and the continuous wavelet transform to look at the major forcing factor of the nutrient utilization variability in the Arctic Ocean. The resolution of the $\delta^{15}N$ time series is uneven. To resolve this issue, we have used Piecewise Cubic Hermite Interpolation to make the data set evenly spaced. They show a significant periodicity of around 130 kyr (Figures 5b and 5c). It matches closely with the eccentricity cycle, which possesses periodicities near 95 and 125 kyr (Laskar et al., 2004). The obliquity and precession cycles are also present though they are not significant (Figure 5). The resolution of the data set ranges from 5 to 11 kyr with an average sampling resolution of ~8,000 years, which allowed us to capture the obliquity and precession cycles (Figure 5). Thus, the dominant forcing factor is the eccentricity cycle. However, the same orbitally paced control (e.g. eccentricity cycle) is observed in oceanic heat inflow into the Arctic (Rahaman et al., 2020). It suggests that enhanced inflow of NAC to the Arctic and the high relative nutrient utilization during warmer periods including MPWP follows the eccentricity cyclicity. The cross wavelet analysis (Figure 5e) shows the common highest power between these two time-series. We have multiplied the ε_{Nd} data with −1 so that it follows the same trend with the $\delta^{15}N$ values without changing the interpretation of water mass circulation. The right-pointing arrows from 3.15 to 2.9 Ma at the eccentricity band show in-phase relation between the enhanced inflow of NAC and the strong stratification (Figure 5e). This result implies that the interglacials with high eccentricity and strong solar insolation in Northern Hemisphere may have resulted in the reduction of sea ice cover. Further, the closure of Arctic gateways (Bering Strait and the Canadian Arctic Archipelago) during MPWP strengthened the AMOC (Otto-Bliesner et al., 2017; Zhang et al., 2020) that could have further enhanced the North Atlantic current to the Arctic that increased the heat transport and subsequent stratification and sea ice melt.

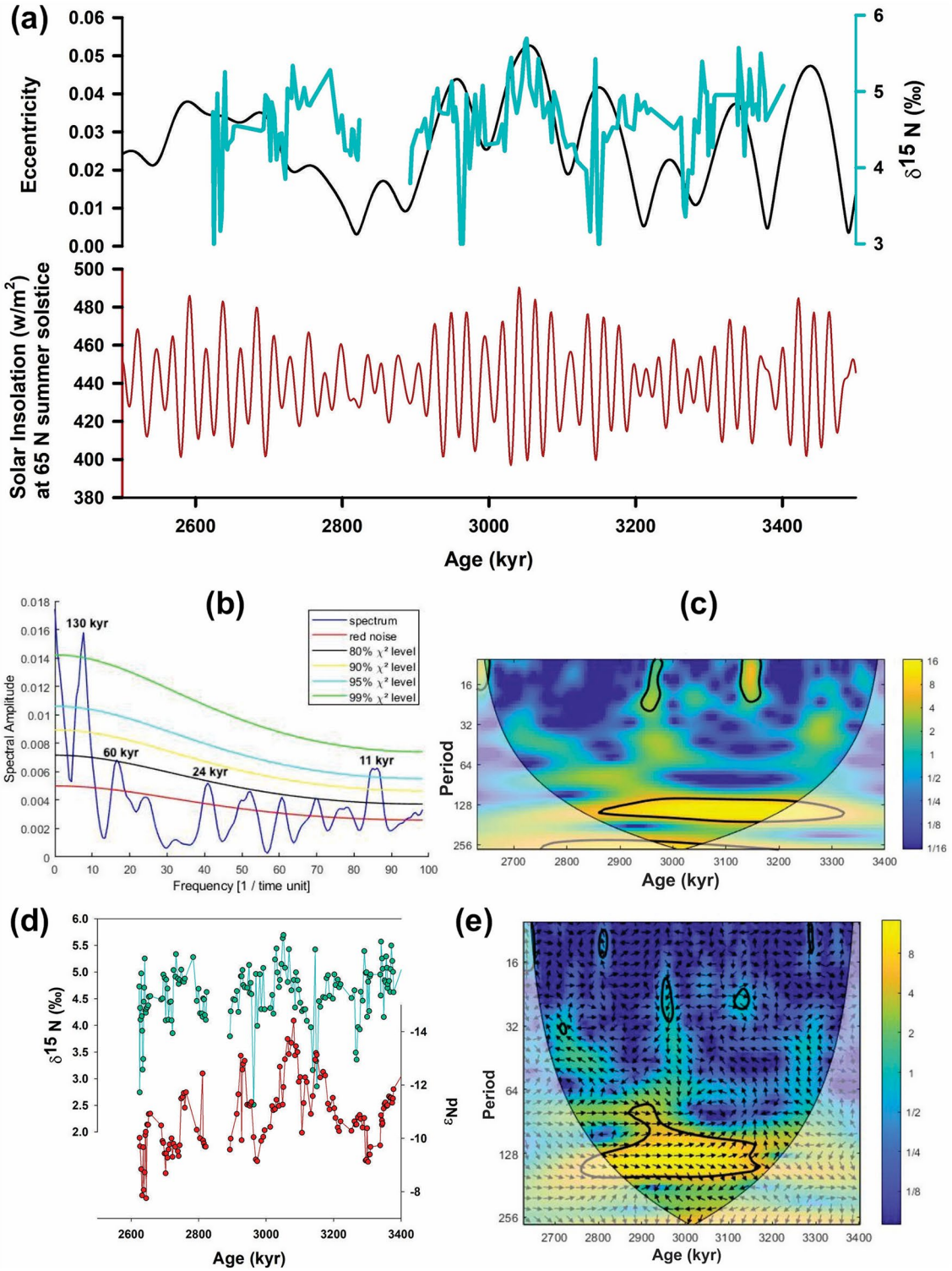

Figure 5. Correlation between orbital forcing and the relative nutrient utilization related to Arctic stratification. (a) Comparison of eccentricity and insolation cycles (Berger & Loutre, 1991) with relative nutrient utilization; (b) and (c) show spectral analysis and continuous wavelet transform for relative nutrient utilization; (d) Comparison between $\delta^{15}N$ (‰) values with authigenic ε_{Nd} indicate that stratification increases during the episodes of enhanced inflow of NAC to the Arctic Ocean; (e) Cross wavelet analysis of two time-series representing Arctic stratification and North Atlantic Current (NAC)-inflow indicating the common highest power. The thick black contour represents the 5% significance level against red noise. The area between the black thin line and the time axis represents the cone of influence. Arrows pointing towards the right show in-phase relation.

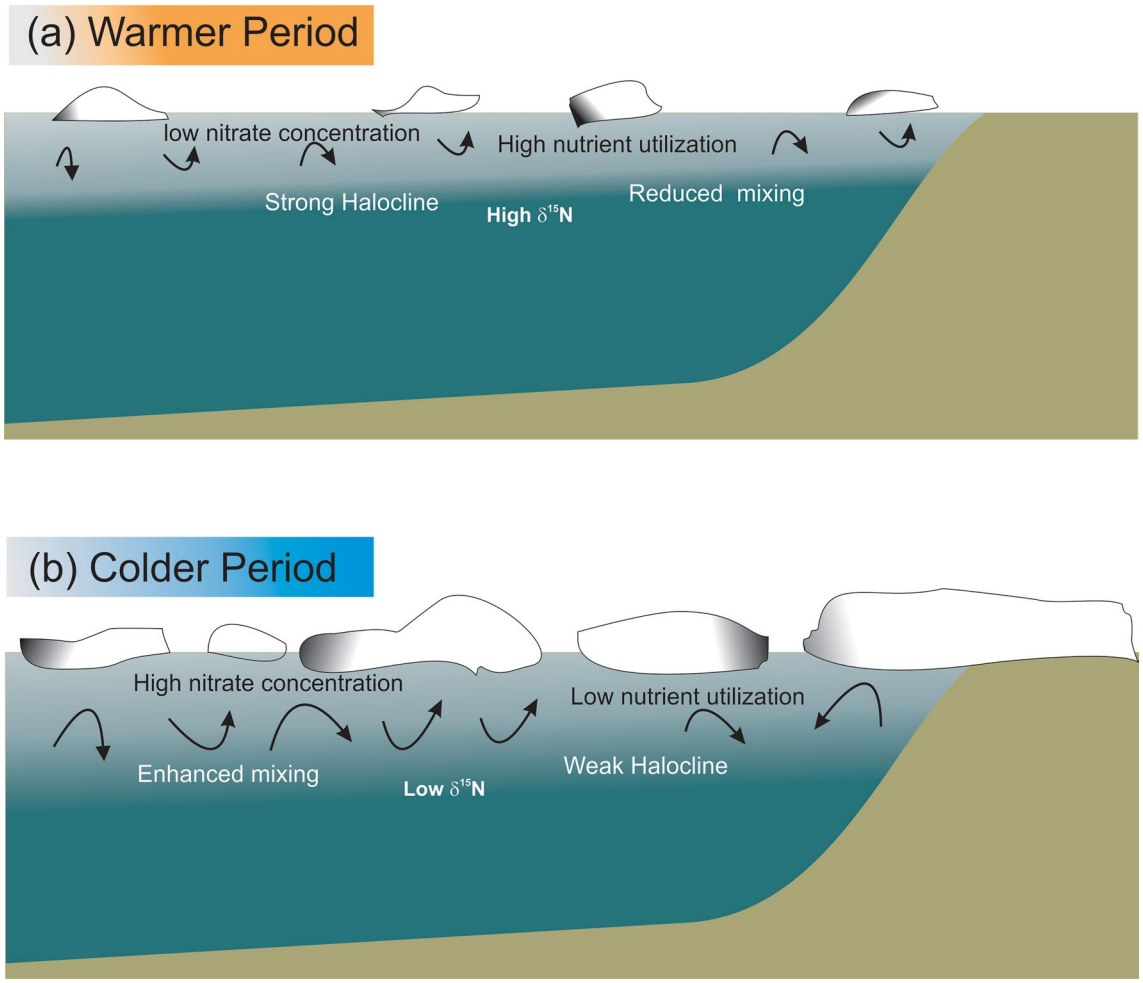

Figure 6. Conceptual representation of stratification at the core site during the late Pliocene. (a) The warmer period is characterized by less sea ice cover at the top (open ocean condition). Fresher surface water is separated from the more saline intermediate water. The reduced mixing is denoted by smaller arrow marks. The stronger stratification inhibits the supply of nutrients to the surface, which results in a high $\delta^{15}N$ value; (b) The colder period is having more sea ice cover at the surface. The brine rejection during the formation of sea ice causes high saline upper surface water. It breaks the stratification formed due to the salinity gradient and causes deeper mixing. Enhanced mixing is represented by bigger arrow marks. It provides nutrients to the surface and which results in a low $\delta^{15}N$ value.

5. Conclusions

We find high relative nutrient utilization in the AAG region indicating low nutrient concentration in the mixed layer during the late Pliocene warm periods including the MPWP. Such oligotrophic conditions developed in response to maximum utilization of available nutrients with no replenishment due to enhanced stratification. The stratification strengthened due to the higher sea ice melt, river discharge, and NAC inflow. Enhanced stratification parallels higher productivity because of sufficient light availability during relatively more ice-free conditions of interglacials. In contrast, low relative nutrient utilization occurred during late Pliocene glacial periods implying high nutrient supply due to reduced stratification and enhanced ocean mixing. The water column stratification variability is predominantly controlled by the eccentricity cycle. Our results imply that during the current scenario of global warming, the enhanced sea ice melt and its internal positive feedbacks can cause strong stratification and upper layer freshening in the near future.

Data Availability Statement

The data used in this study can be accessed from Mendeley Data (https://data.mendeley.com/datasets/g54vtzmtjd/1).

Acknowledgment
We thank the Secretary, Ministry of Earth Sciences (MoES) and Director, National Center for Polar and Ocean Research (NCPOR Contribution no. J-10/2021-22) for support. This research is supported by the MoES, Govt. of India (MoES/Ind-Nor/PS-8/2015) and Research Council of Norway (Grant No. 248793, 223259) through the INDNOR program. We also thank the PACT (Pliocene Arctic Climate Teleconnection) project colleagues for sharing the samples and the data.

References

Aagaard, K., Coachman, L. K., & Carmack, E. (1981). On the halocline of the Arctic Ocean. *Deep Sea Research Part A, Oceanographic Research Papers*, *28*(6), 529–545. https://doi.org/10.1016/0198-0149(81)90115-1

Adkins, J. F., McIntyre, K., & Schrag, D. P. (2002). The salinity, temperature, and δ18O of the glacial deep ocean. *Science*, *298*, 1769–1773. https://doi.org/10.1126/science.1076252

Altabet, M. A., & Francois, R. (1994). Sedimentary nitrogen isotopic ratio as a recorder for surface ocean nitrate utilization. *Global Biogeochemical Cycles*, *8*, 103–116. https://doi.org/10.1029/93GB03396

Bartoli, G., Hönisch, B., & Zeebe, R. E. (2011). Atmospheric CO_2 decline during the Pliocene intensification of Northern Hemisphere glaciations. *Paleoceanography*, *26*(4), 1–14. https://doi.org/10.1029/2010PA002055

Berends, C. J., De Boer, B., Dolan, A. M., Hill, D. J., & Van De Wal, R. S. W. (2019). Modeling ice sheet evolution and atmospheric CO_2 during the Late Pliocene. *Climate of the Past*, *15*, 1603–1619. https://doi.org/10.5194/cp-15-1603-2019

Berger, A., & Loutre, M. F. (1991). Insolation values for the climate of the last 10 million years. *Quaternary Science Reviews*, *10*(4), 297–317. https://doi.org/10.1016/0277-3791(91)90033-Q

Beszczynska-Mller, A., Fahrbach, E., Schauer, U., & Hansen, E. (2012). Variability in Atlantic water temperature and transport at the entrance to the Arctic Ocean, 1997-2010. *ICES Journal of Marine Science*, *69*, 852–863. https://doi.org/10.1093/icesjms/fss056

Brodie, C. R., Casford, J. S. L., Lloyd, J. M., Leng, M. J., Heaton, T. H. E., Kendrick, C. P., & Yongqiang, Z. (2011). Evidence for bias in C/N, δ13C and δ15N values of bulk organic matter, and on environmental interpretation, from a lake sedimentary sequence by pre-analysis acid treatment methods. *Quaternary Science Reviews*, *30*(21–22), 3076–3087. https://doi.org/10.1016/j.quascirev.2011.07.003

Carmack, E., Polyakov, I., Padman, L., Fer, I., Hunke, E., Hutchings, J., et al. (2015). Toward quantifying the increasing role of oceanic heat in sea ice loss in the new arctic. *Bulletin of the American Meteorological Society*, *96*(12), 2079–2105. https://doi.org/10.1175/BAMS-D-13-00177.1

Cavalieri, D. J., & Parkinson, C. L. (2012). Arctic sea ice variability and trends, 1979-2010. *The Cryosphere*, *6*(4), 881–889. https://doi.org/10.5194/tc-6-881-2012

Coachman, L. K., & Barnes, C. A. (1962). Surface Water in the Eurasian Basin of the Arctic Ocean. *Arctic*, *15*(4). https://doi.org/10.14430/arctic3581

Codispoti, L. A., Kelly, V., Thessen, A., Matrai, P., Suttles, S., Hill, V., et al. (2013). Synthesis of primary production in the Arctic Ocean: III. Nitrate and phosphate based estimates of net community production. *Progress in Oceanography*, *110*, 126–150. https://doi.org/10.1016/j.pocean.2012.11.006

Cronin, T. M., Whatley, R., Wood, A., Tsukagoshi, A., Ikeya, N., Brouwers, E. M., & Briggs, W. M. (1993). Microfaunal evidence for elevated Pliocene temperatures in the Arctic Ocean. *Paleoceanography*, *8*, 161–173. https://doi.org/10.1029/93PA00060

de la Vega, E., Chalk, T. B., Wilson, P. A., Bysani, R. P., & Foster, G. L. (2020). Atmospheric CO_2 during the Mid-Piacenzian warm period and the M2 glaciation. *Scientific Reports*, *10*(1), 14–21. https://doi.org/10.1038/s41598-020-67154-8

De Schepper, S., Groeneveld, J., Naafs, B. D. A., Van Renterghem, C., Hennissen, J., Head, M. J., et al. (2013). Northern hemisphere glaciation during the globally warm early late Pliocene. *PloS One*, *8*(12), e81508. https://doi.org/10.1371/journal.pone.0081508

de Steur, L., Hansen, E., Gerdes, R., Karcher, M., Fahrbach, E., & Holfort, J. (2009). Freshwater fluxes in the East Greenland Current: A decade of observations. *Geophysical Research Letters*, *36*, L23611. https://doi.org/10.1029/2009GL041278

Dowsett, H. J., Cronin, T. M., Poore, R. Z., Thompson, R. S., Whatley, R. C., & Wood, A. M. (1992). Micropaleontological evidence for increased meridional heat transport in the North Atlantic ocean during the Pliocene. *Science*, *258*(5085), 1133–1135. https://doi.org/10.1126/science.258.5085.1133

Dowsett, H. J., Robinson, M. M., & Foley, K. M. (2009). Pliocene three-dimensional global ocean temperature reconstruction. *Climate of the Past*, *5*(4), 769-783.

Dowsett, H. J., Robinson, M. M., Foley, K. M., Herbert, T. D., Otto-Bliesner, B. L., & Spivey, W. (2019). The mid-Piacenzian of the North Atlantic Ocean. *Stratigraphy*, *16*(3), 119–144. https://doi.org/10.29041/strat.16.3.119-144

Dymond, J., Suess, E., & Lyle, M. (1992). Correction to "Barium in the deep-sea sediment: A geochemical proxy for paleoproductivity". *Paleoceanography*, *7*(3), 391. https://doi.org/10.1029/92PA01080

Freudenthal, T., Wagner, T., Wenzhöfer, F., Zabel, M., & Wefer, G. (2001). Early diagenesis of organic matter from sediments of the Eastern subtropical Atlantic: Evidence from stable nitrogen and carbon isotopes. *Geochimica et Cosmochimica Acta*, *65*(11), 1795–1808. https://doi.org/10.1016/S0016-7037(01)00554-3

Gingele, F. X., Zabel, M., Kasten, S., Bonn, W. J., & Nürnberg, C. C. (1999). Biogenic Barium as a Proxy for Paleoproductivity: Methods and Limitations of Application. *Use of Proxies in Paleoceanography*, 345–364. https://doi.org/10.1007/978-3-642-58646-0_13

Gleick, P. H. (2000). *The world's water 2000– 2001* (pp. 39–61). Island Press.

Haugan, P. M. (1999). Structure and heat content of the West Spitsbergen Current. *Polar Research*, *18*, 183–188. https://doi.org/10.1111/j.1751-8369.1999.tb00291.x

Haywood, A. M., Hill, D. J., Dolan, A. M., Otto-Bliesner, B. L., Bragg, F., Chan, W. L., et al. (2013). Large-scale features of Pliocene climate: Results from the Pliocene model intercomparison project. *Climate of the Past*, *9*, 191–209. https://doi.org/10.5194/cp-9-191-2013

Haywood, A. M., Tindall, J. C., Dowsett, H. J., Dolan, A. M., Foley, K. M., Hunter, S. J., et al. (2020). The Pliocene model intercomparison project phase 2: Large-scale climate features and climate sensitivity. *Climate of the Past*, *16*(6), 2095–2123. https://doi.org/10.5194/cp-16-2095-2020

Knies, J., Brookes, S., & Schubert, C. J. (2007). Re-assessing the nitrogen signal in continental margin sediments: New insights from the high northern latitudes. *Earth and Planetary Science Letters*, *253*(3–4), 471–484. https://doi.org/10.1016/j.epsl.2006.11.008

Knies, J., Cabedo-Sanz, P., Belt, S. T., Baranwal, S., Fietz, S., & Rosell-Melé, A. (2014). The emergence of modern sea ice cover in the Arctic Ocean. *Nature Communications*, *5*, 1–7. https://doi.org/10.1038/ncomms6608

Knies, J., Matthiessen, J., Vogt, C., & Stein, R. (2002). Evidence of "Mid-Pliocene (similar to 3 Ma) global warmth" in the eastern Arctic Ocean and implications for the Svalbard/Barents Sea ice sheet during the late Pliocene and early Pleistocene (similar to 3-1.7 Ma). *Boreas*, *31*(1), 82–93. https://doi.org/10.1080/03009480210652

Laskar, J., Robutel, P., Joutel, F., Gastineau, M., Correia, A. C. M., & Levrard, B. (2004). A long-term numerical solution for the insolation quantities of the Earth. *Astronomy and Astrophysics*, *428*, 261–285. https://doi.org/10.1051/0004-6361:20041335

Lawrence, K. T., Herbert, T. D., Brown, C. M., Raymo, M. E., & Haywood, A. M. (2009). High-amplitude variations in north atlantic sea surface temperature during the early pliocene warm period. *Paleoceanography*, *24*(2), PA2218. https://doi.org/10.1029/2008PA001669

Lisiecki, L. E., & Raymo, M. E. (2005). A Pliocene-Pleistocene stack of 57 globally distributed benthic δ18O records. *Paleoceanography*, *20*(1), PA1003. https://doi.org/10.1029/2004PA001071

Lourens, L. J., Sluijs, A., Kroon, D., Zachos, J. C., Thomas, E., Röhl, U., et al. (2005). Astronomical pacing of late Palaeocene to early Eocene global warming events. *Nature*, *435*(7045), 1083-1087.

Meyers, P. A. (1994). Preservation of elemental and isotopic source identification of sedimentary organic matter. *Chemical Geology*, *114*, 289–302. https://doi.org/10.1016/0009-2541(94)90059-0

Myhre, A. M., Thiede, J., & Firth, J. V. (1995). Proceedings of the Ocean Drilling Program. In *Scientific Results*, *151*, 221–270.

Nummelin, A., Ilicak, M., Li, C., & Smedsrud, L. H. (2016). Consequences of future increased Arctic runoff on Arctic Ocean stratification, circulation, and sea ice cover. *Journal of Geophysical Research: Oceans*, *121*, 617–637. https://doi.org/10.1002/2015JC011156

Onarheim, I. H., Smedsrud, L. H., Ingvaldsen, R. B., & Nilsen, F. (2014). Loss of sea ice during winter north of Svalbard. *Tellus, Series A: Dynamic Meteorology and Oceanography*, *66*(1), 23933. https://doi.org/10.3402/tellusa.v66.23933

Otto-Bliesner, B. L., Jahn, A., Feng, R., Brady, E. C., Hu, A., & Löfverström, M. (2017). Amplified North Atlantic warming in the late Pliocene by changes in Arctic gateways. *Geophysical Research Letters*, *44*(2), 957–964. https://doi.org/10.1002/2016GL071805

Peralta-Ferriz, C., & Woodgate, R. A. (2015). Seasonal and interannual variability of pan-Arctic surface mixed layer properties from 1979 to 2012 from hydrographic data, and the dominance of stratification for multiyear mixed layer depth shoaling. *Progress in Oceanography*, *134*, 19–53. https://doi.org/10.1016/j.pocean.2014.12.005

Perovich, D. K., Richter-Menge, J. A., Jones, K. F., Light, B., Elder, B. C., Polashenski, C., et al. (2011). Arctic sea-ice melt in 2008 and the role of solar heating. *Annals of Glaciology*, *52*(57), 355–359. https://doi.org/10.3189/172756411795931714

Pnyushkov, A. V., Polyakov, I. V., Ivanov, V. V., Aksenov, Y., Coward, A. C., Janout, M., & Rabe, B. (2015). Structure and variability of the boundary current in the Eurasian Basin of the Arctic Ocean. *Deep-Sea Research Part I Oceanographic Research Papers*, *101*, 80–97. https://doi.org/10.1016/j.dsr.2015.03.001

Polyakov, I. V., Pnyushkov, A. V., Alkire, M. B., Ashik, I. M., Baumann, T. M., Carmack, E. C., et al. (2017). Greater role for Atlantic inflows on sea-ice loss in the Eurasian Basin of the Arctic Ocean. *Science*, *356*(6335), 285–291. https://doi.org/10.1126/science.aai8204

Rahaman, W., Smik, L., Köseoğlu, D., N, L., Tarique, M., Thamban, M., et al. (2020). Reduced Arctic sea ice extent during the mid-Pliocene warm period concurrent with increased Atlantic-climate regime. *Earth and Planetary Science Letters*, *550*, 116535. https://doi.org/10.1016/j.epsl.2020.116535

Randelhoff, A., Sundfjord, A., & Reigstad, M. (2015). Seasonal variability and fluxes of nitrate in the surface waters over the Arctic shelf slope. *Geophysical Research Letters*, *42*(9), 3442–3449. https://doi.org/10.1002/2015GL063655

Ravelo, A. C., & Andreasen, D. H. (2000). Enhanced circulation during a warm period. *Geophysical Research Letters*, *27*(7), 1001–1004. https://doi.org/10.1029/1999GL007000

Robinson, M. M. (2009). New quantitative evidence of extreme warmth in the Pliocene Arctic. *Stratigraphy*, *6*(4), 265–276.

Robinson, R. S., Kienast, M., Luiza Albuquerque, A., Altabet, M., Contreras, S., De Pol Holz, R., et al. (2012). A review of nitrogen isotopic alteration in marine sediments. *Paleoceanography*, *27*(4). https://doi.org/10.1029/2012PA002321

Rohling, E. J., Foster, G. L., Grant, K. M., Marino, G., Roberts, A. P., Tamisiea, M. E., & Williams, F. (2014). Sea-level and deep-sea-temperature variability over the past 5.3 million years. *Nature*, *508*, 477–482. https://doi.org/10.1038/nature13230

Rudels, B. (2015). Arctic Ocean circulation, processes and water masses: A description of observations and ideas with focus on the period prior to the International Polar Year 2007-2009. *Progress in Oceanography*, *132*, 22–67. https://doi.org/10.1016/j.pocean.2013.11.006

Rudels, B., Larsson, A., & Sehlstedt, P. (1991). Stratification and water mass formation in the Arctic Ocean: Some implications for the nutrient distribution. *Polar Research*, *10*(1), 19–32. https://doi.org/10.3402/polar.v10i1.6724

Ruttenberg, K. C., & Goñi, M. A. (1997). Phosphorus distribution, C:N:P ratios, and δ13C(OC) in arctic, temperate, and tropical coastal sediments: Tools for characterizing bulk sedimentary organic matter. *Marine Geology*, *139*(1–4), 123–145. https://doi.org/10.1016/S0025-3227(96)00107-7

Sato, T., & Kameo, K. (1996). Pliocene to Quaternary Calcareous Nannofossil Biostratigraphy of the Arctic Ocean, with Reference to Late Pliocene Glaciation. In *Proceedings of the Ocean Drilling Program*, 151, *Scientific Results*, 39–59. https://doi.org/10.2973/odp.proc.sr.151.112.1996

Schubert, C. J., & Calvert, S. E. (2001). Nitrogen and carbon isotopic composition of marine and terrestrial organic matter in Arctic Ocean sediments: Implications for nutrient utilization and organic matter composition. *Deep-Sea Research Part I Oceanographic Research Papers*, *48*(3), 789–810. https://doi.org/10.1016/S0967-0637(00)00069-8

Schubert, C. J., Stein, R., & Calvert, S. E. (2001). Tracking nutrient and productivity variations over the last deglaciation in the Arctic Ocean. *Paleoceanography*, *16*(2), 199–211. https://doi.org/10.1029/2000PA000503

Sévellec, F., Fedorov, A. V., & Liu, W. (2017). Arctic sea-ice decline weakens the Atlantic Meridional Overturning Circulation. *Nature Climate Change*, *7*, 604–610. https://doi.org/10.1038/NCLIMATE3353

Sigman, D., Karsh, K., & Casciotti, K. (2009). Ocean process tracers: Nitrogen isotopes in the ocean. *Encyclopedia of Ocean Sciences*, 40–54. https://doi.org/10.1006/rwos.2001.0172

Tan, N., Ramstein, G., Dumas, C., Contoux, C., Ladant, J. B., Sepulchre, P., et al. (2017). Exploring the MIS M2 glaciation occurring during a warm and high atmospheric CO_2 Pliocene background climate. *Earth and Planetary Science Letters*, *472*, 266–276. https://doi.org/10.1016/j.epsl.2017.04.050

Thibodeau, B., Bauch, H. A., & Pedersen, T. F. (2017). Stratification-induced variations in nutrient utilization in the Polar North Atlantic during past interglacials. *Earth and Planetary Science Letters*, *457*, 127–135. https://doi.org/10.1016/j.epsl.2016.09.060

Torres-Valdés, S., Tsubouchi, T., Bacon, S., Naveira-Garabato, A. C., Sanders, R., McLaughlin, F. A., et al. (2013). Export of nutrients from the Arctic Ocean. *Journal of Geophysical Research: Oceans*, *118*(4), 1625–1644. https://doi.org/10.1002/jgrc.20063

Tripathi, S., Tiwari, M., Lee, J., Khim, B. K., Pandey, D. K., Clift, P. D., et al. (2017). First evidence of denitrification vis-à-vis monsoon in the Arabian Sea since late Miocene. *Scientific Reports*, *7*, 1–7. https://doi.org/10.1038/srep43056

Zhang, Z., Li, X., Guo, C., Otterå, O. H., Nisancioglu, K., Tan, N., et al. (2020). Mid-Pliocene Atlantic Meridional overturning circulation simulated in PlioMIP2. *Climate of the Past Discussions*, *17*(1), 529–543. https://doi.org/10.5194/cp-2020-120